2024 European Control Conference (ECC)
June 25-28, 2024. Stockholm, Sweden

Model-free based pitch control of a wind turbine blade section: aerodynamic simulation

Loïc Michel[1], Emmanuel Guilmineau[2], Caroline Braud[2], Franck Plestan[1], Jean-Pierre Barbot[1 3]

Abstract— **This work addresses the problem of controlling the local aerodynamic lift of a wind turbine blade taking into account disturbances caused by turbulent perturbations at the blade scale. This work deals with the study of a model-free based control algorithm implemented in the high fidelity simulated environment ISIS-CFD, where the controller acts at the level of the blade section to track the lift to a desired reference. Numerical experiments have been conducted in order to highlight some properties of the aerodynamic closed-loop system under several operating conditions.**

I. Introduction

To optimize the energy extraction from the wind while minimizing rotor loads and thus increasing lifetime of wind turbines, the control is generally performed globally without considering the local aerodynamics around the blade. The indirect measure of the lift, through a limited number of wall pressure sensors, can be an alternative solution to control the power extracted from the wind at the blade scale. This interest is also emphasized knowing that the wind inflow interaction with blade aerodynamics can lead to power loss, load fluctuations and noise generation (see e.g. [1] [2]).

This study deals with the development of a control algorithm, operating at the level of the blade section and taking into account disturbances caused by turbulent inflows [3], the control objective being to track to a desired lift reference by driving the pitch angle of the blade. The investigations have been made in a high fidelity simulated environment using a numerical model solving Navier-Stokes equations: the ISIS-CFD solver [4].

Blade pitch control has received recently a lot of attention. Particularly, as stated in [5], individual pitch controller is preferred to cope with structural load reduction for which advanced control methods have been proposed. Strategies based on learning methods such as neural networks and reinforcement have been proposed e.g. in [6], [7], iterative learning control in [8], neural based PID controllers in [9], feed-forward model predictive control, in [10], and adaptive high order sliding-mode controller [11]. The direct control of the blade using local inflow measurements has been studied in [12] and cascaded controllers has been proposed in [13].

The ISIS-CFD solver provides a very precise / high fidelity numerical model based on the complete Navier-Stokes equations. Such coupling between control laws and numerical CFD remains a very challenging task since the control has to deal with an unknown and uncertain complex model. The major issue in extracting a simple dynamical model from unsteady aerodynamic flows leads to consider a "model-free" type of control law, for which numerical experiments have been conducted in order to highlight some performances properties of the aerodynamic closed-loop system under several operating conditions. The objective of this study is to evaluate the performances of the lift control in order to draw experimental perspectives that will be performed at a full chord scale.

Taking into account the difficulty to model phenomena in aerodynamics, and, in particular, to model the flow around the blade environment, a model-free based control technique has been implemented to drive the pitch angle of the blade in order to track the simulated lift closed to a reference. Our investigations focus on online model-free based control methods that do not involve machine learning strategies for which a huge number of simulations are requested. For accurate results, at least a thousand of results is necessary taking into account that a typical simulation requires a couple of days to be processed on a "standard" computer[1]. However, machine learning would be efficient to deal with the particular tuning of model-based controller.

The paper is organized as follow: Section II presents the methodology of the numerical setup including the presentation of the ISIS-CFD solver and the proposed model-free based control. Section III depicts the results of the numerical experiments. Section IV discusses the efficiency of the proposed lift controller. Section V gives some concluding and perspective remarks.

II. Methodology

A. The ISIS-CFD solver

The in-house solver ISIS-CFD developed by CNRS and Centrale Nantes, also available as a part of the FINE™/Marine computing suite worldwide distributed by Cadence Design Systems, is an incompressible multiphase unsteady Reynolds-averaged Navier-Stokes (URANS) solver

This work has been partially supported by ANR (*Agence Nationale de la Recherche*) with project CREATIF ANR-20-CE05-0039, by the WEAMEC project "FOWTBLADE" Pays-de-la-Loire regional project and by the GOWIBA project that is funded by the Carnot Instute Marine Engineering Research for Sustainable, Safe and Smart Seas. Jean-Pierre Barbot is supported with (*Région Pays de la Loire*) Connect Talent GENYDROGENE project.

[1]Loïc Michel, Franck Plestan and Jean-Pierre Barbot are with Nantes Université, Ecole Centrale Nantes, CNRS, LS2N, UMR 6004, 44000 Nantes, France (e-mail: {loic.michel, franck.plestan}@ec-nantes.fr).

[2]Emmanuel Guilmineau and Caroline Braud are with Nantes Université, Ecole Centrale Nantes, CNRS, LHEEA, UMR 6598, 44000 Nantes, France (e-mail: {emmanuel.guilmineau, caroline.braud}@ec-nantes.fr).

[3]Jean-Pierre Barbot is also with ENSEA, Quartz Laboratory, EA 7393, 95014 Cergy-Pontoise, France (e-mail: barbot@ensea.fr).

[1]For example an Intel® Core™ i7 with 260 Go of RAM.

Copyright ©2024 EUCA

mainly devoted to marine hydrodynamics. It is based on a fully-unstructured (face-based) finite volume discretization with specific functionalities needed for multiphase flows and industrial applications [4], [14]. Within this framework, the incompressible conservation laws under isothermal conditions, are written as:

$$\frac{\partial}{\partial t}\int_V \rho dV + \int_S \rho(U_i - U_{d_i})\cdot n_i dS = 0 \tag{1}$$

$$\frac{\partial}{\partial t}\int_V \rho U_i dV + \int_S \rho U_i(U_j - U_{d_j})\cdot n_j dS = \int_S (\tau_{ij} - p)\cdot n_j dS \tag{2}$$

where V is the domain of interest, or control volume, bounded by the closed surface S, with a unit normal vector n_i directed outward, moving at the displacement velocity U_{d_i}, which corresponds to the mesh motion. U_i and p represent, respectively, the flow velocity and pressure fields. ρ is the density of the fluid and τ_{ij} are the component of the stress tensor.

The method features several sophisticated turbulence models: apart from the classical two-equation k-ϵ and k-ω models, the anisotropic two-equation Explicit Algebraic Reynolds Stress Model (EARSM), as well as Reynolds Stress Transport Models, are available. All models are available with wall-function or low-Reynolds near wall formulations. Hybrid RANS/LES turbulence models based on Detached Eddy Simulation (DES-SST, DDES-SST, IDDES-SST) are also implemented and have been thoroughly validated on automotive flows characterized by large separations [15] and ships at steady drift [16]. Moreover, the solver accepts sliding and overset grids and features an anisotropic adaptive grid refinement functionality [17], [18] applied to unstructured hexahedral meshes.

All variables are stored at the geometric center of arbitrary shaped cells. Volume and surface integrals are evaluated with second-order accurate approximations. Numerical fluxes are reconstructed on mesh faces by linear extrapolation of integrand from the neighboring cell centers. A centered scheme is used for the diffusion terms, whereas the convective fluxes, the scheme implemented in the ISIS-CFD code is the AVLSMART scheme [19]. The velocity filed is obtained form the momentum conservation equations, and the pressure field is extracted from the mass conservation constraint, or continuity equation, transformed into a pressure equation. The pressure equation is obtained in the spirit of Rhie and Chow [20]. Momentum and pressure equations are solved in a segregated manner as in the SIMPLE coupling procedure [21]. A second-order backward difference scheme is used to discretize time.

B. A model-free based control law

The model-free control approach [22] can be considered as an alternative to usual controls and model-driven or neural network based controllers, as it does not need any prior knowledge of the plant or huge database, and it is straightforward to tune, contrary to the commonly used classic PID controllers whose tuning usually depends on trial and error methods. A modified version of the model-free control approach has been proposed in [23] as an integrator including a forgetting factor

$$u_k = \Psi_k \,.\int_0^t K_i(y_k^* - y_k)\,d\tau \tag{3}$$

where k is the discrete iteration index and Ψ_k is a time series that "adjusts" online the gain of the integrator in (1)

$$\Psi_k = \Psi_{k-1} + K_p(K_\alpha e^{-K_\beta . k} - y_k) \tag{4}$$

In (3)-(4), u_k is the control output ; y_k^* is the output reference trajectory; y_k is the output of the controlled system; K_p, K_I, K_α and K_β are real positive tuning gains.

Remark that in (3), in order to minimize the influence of measurement noise, no output numerical derivative is used, and only an integral term appears, which is very favorable in terms of minimizing the influence of measurement noise. In fact, integration of the noisy output y_k is only sensible to the noise average. For example, this approach is in line with that of ALIEN differentiator [24], where integration terms are used to avoid problem on differentiation of noisy signal. Moreover, roughly speaking, in equation (4), there is a memory effect with the term Ψ_{k-1} and a forgetting target factor generated by the exponential function $K_\alpha e^{-K_\beta . k}$.

C. Coupling between control and flow solver

The lift tracking is achieved through a control loop wherein the control input of the system (actuator + blade) is a DC motor. Figure 1 presents the scheme of the proposed discrete closed-loop where the control is sampled at $T_s = 0.2$ ms within the ISIS-CFD solver: u_k is the control input (voltage applied to the DC motor), α_k is the pitch angle and F_k is the lift force given by the ISIS-CFD solver. The DC motor, that drives the blade pitch angle, is modelled as a first order transfer function of time constant $\tau = 0.5$ s.

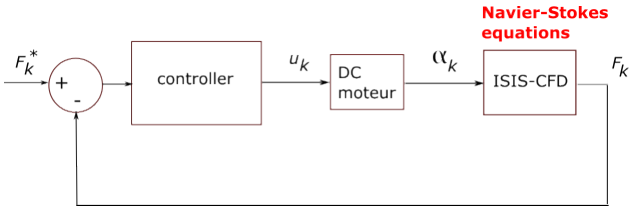

Fig. 1: Schematic of the control loop for lift tracking

III. Numerical results and discussion

A. Blade characterisation

The 2D blade section used during the simulations is shown in Fig. 2. The shape of the profile is derived by scanning the blade of a 2-MW commercial wind turbine. The extracted 2D blade section is located at 80% of the rotor radius. The chord length C is 1.25 m.

In this study, the k-ω SST turbulence model [25] is used. Several wind velocities, U_∞, which are imposed at the inlet of the computational domain, are investigated: from 28.4

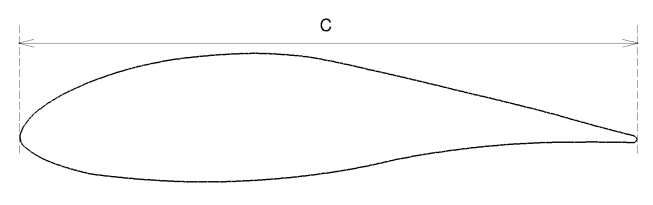

Fig. 2: Geometry of the blade section

ms^{-1} to 56.7 ms^{-1} which leads to the Reynolds number, Re = $\rho U_\infty C/\mu$, from 2.35×10^6 to 4.70×10^6, respectively. The Reynolds number is a dimensionless quantity that helps predict fluid flow patterns in different situations by measuring the ratio between inertial and viscous forces; μ is the dynamic viscosity.

The first step is the characterisation of the flow for different pitch angles and Reynolds numbers, in order to have an idea about the lift force range. Figure 3 shows the evolution of the lift force and the lift coefficient, $Cl = F_y/(\frac{1}{2}\rho U_\infty^2 C)$, where F_y is the lift force, versus the pitch angle with respect to two particular Reynolds numbers. The lift coefficient is a dimensionless quantity of the lift force. The change in Reynolds number, and therefore in wind velocity at the inlet, has a limited effect on the lift coefficient, that remains in the same range. Remark that, the values of the lift coefficient are similar between both Reynolds numbers but the values of the lift force are of different range. These simulations give an idea of the values of lift force and lift coefficient that can be obtained for different Reynolds numbers.

B. Tracking of a constant reference of lift force with a constant wind velocity

All the following simulations start from the solution obtained for the zero pitch angle. The gains of the control law are set to $K_i = 0.1$, $K_p = 1$, $K_\alpha = 1000$ and $K_\beta = 10$.

In this first test case, the objective is to maintain the lift force F_y constant during the whole simulation, with the wind velocity set to 56.7 ms^{-1} (corresponding to Re = 4.70×10^6). The first case sets F_y^* = 1500 N (Cl = 0.75) in Fig. 4. Regarding the second case, the constant lift reference is considered at F_y^* = 3000 N (Cl = 1.24) in Fig. 5.

The results show a tracking and stabilization in both simulations where the predicted lift by the CFD converge to the references. In particular, the pitch angle is 1.43^o for $F_y^* = 1500$ N and 7.64^o for $F_y^* = 3000$ N. These results are in accordance with the Cl curves in Fig. 3.

C. Tracking of a constant reference of lift coefficient with a change of the wind velocity

In this test case, the objective is to maintain Cl constant involving a change of the wind velocity at the inlet. The change of the velocity implies to change also the lift force reference F_y^* in order to hold the lift coefficient Cl = 1.24 at the same value during the whole simulation. The wind velocity is set initially to 56.7 ms^{-1} and is changed at $t = 40$ s to 28.4 ms^{-1} (see Fig. 6).

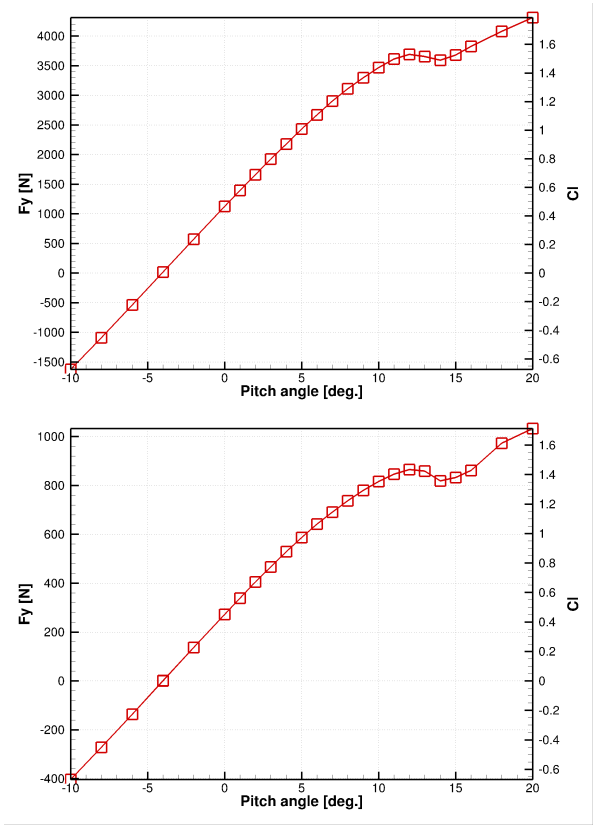

Fig. 3: Evolution of lift force and lift coefficient versus the pitch angle for two Reynolds numbers Re = 4.70×10^6, U_∞ = 56.7. ms^{-1} (top) and Re = 2.35×10^6, U_∞ = 28.4. ms^{-1} (bottom)

Figure 7 illustrates the tracking of the lift force converging to the 3000 N firstly, and then converges to 750 N after the change of the wind velocity. The pitch angle is stabilized first to 7.64^o (3000 N) and then moves to 8.16^o (750 N). These results are in accordance with Fig. 3 where the evolution of the lift force and the lift coefficient are presented with respect to pitch angle for two Reynolds numbers.

D. Tracking of a constant reference of lift force with a perturbation at the wind velocity

In this test case[2], the goal is to maintain the lift force constant taking into account a time-variation of the wind velocity. The reference lift force F_y^* is set to 1350 N. The initial wind velocity is set to 42.5 ms^{-1}. The evolution of the wind velocity is presented in Fig. 8 where the perturbation is applied from $t = 32$ s. to 48 s. The lift tracking under this perturbation is illustrated in Fig. 9 where the pitch angle decreases when the wind velocity increases to maintain the lift force constant. When the the wind velocity decreases, the pitch angle increases again to reach its initial value.

[2]A video that illustrates the simulation is available at https://box.lheea.ec-nantes.fr/index.php/s/6WrOpYwJcBU1IDA.

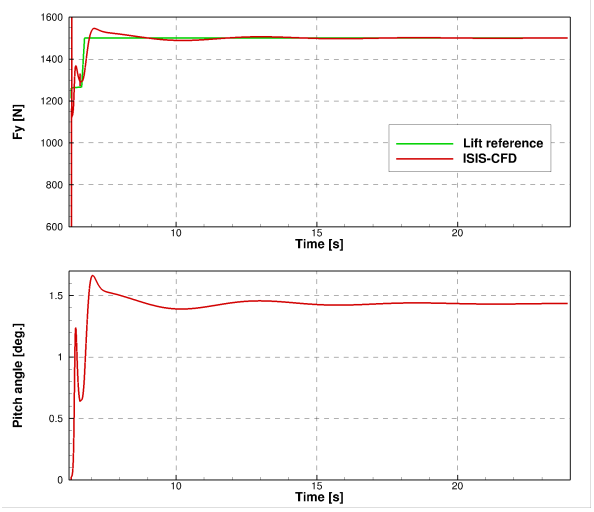

Fig. 4: F_y^* = 1500 N, Re = 4.70×10^6, U_∞ = 56.7. ms^{-1}: Evolution of lift force (top) and pitch angle (bottom) versus the time

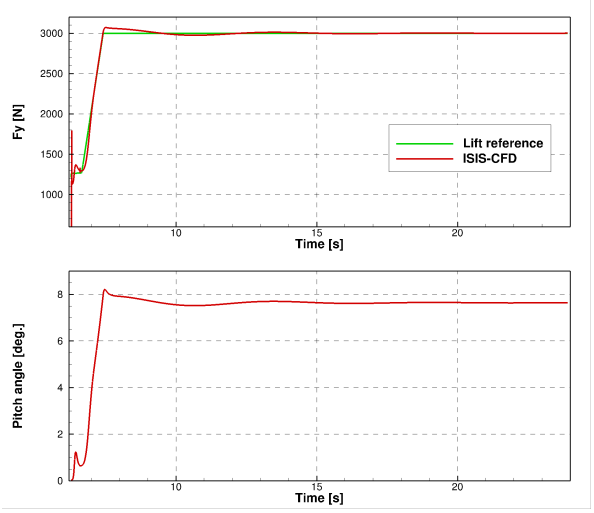

Fig. 5: F_y^* = 3000 N, Re = 4.70×10^6, U_∞ = 56.7. ms^{-1}: Evolution of lift force (top) and pitch angle (bottom) versus the time

E. Tracking of a sinusoidal lift force

The goal, in this last test case, is to evaluate the dynamic tracking response of the control subjected to a sine reference under several frequencies. Roughly speaking, this corresponds to input-output frequency analysis for two wind velocities.

Two sine references are considered: $F_y^* = 3000 + 200 \times \sin(2\pi ft)$ N (wind velocity of 56.7 ms^{-1}) and $F_y^* = 750 + 50 \times \sin(2\pi ft)$ N (wind velocity of 28.4 ms^{-1}).

The tracking of the lift considering the wind velocity of 56.7 ms^{-1} and 28.4 ms^{-1} are illustrated respectively in Fig. 10 and Fig. 11 with respect to a frequency of 1 Hz.

The frequential response of the dynamic of the lift in closed-loop is computed from 0.01 Hz to 20 Hz. A comparison of Fig. 10 and 11 shows that the frequency response

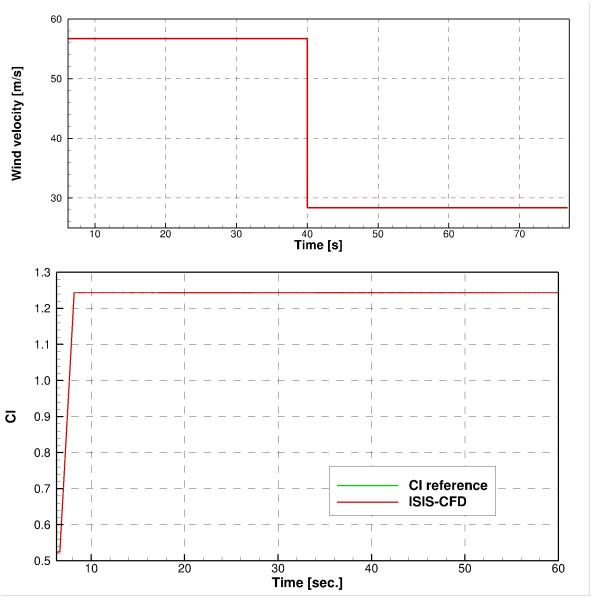

Fig. 6: Cl = 1.4, U_∞ = 56.7 ms^{-1} to 28.4 ms^{-1}: Evolution of the wind velocity (top) and the lift coefficient (bottom) versus the time

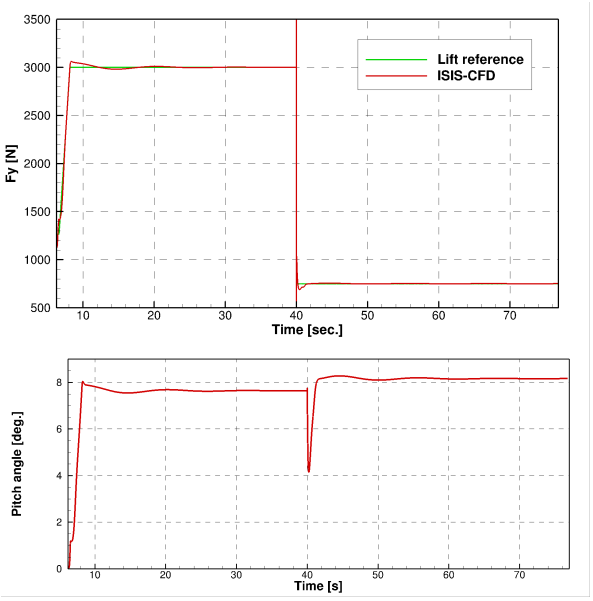

Fig. 7: Cl = 1.4, U_∞ = 56.7 ms^{-1} to 28.4 ms^{-1}: Evolution of lift force (top) and pitch angle (bottom) versus the time

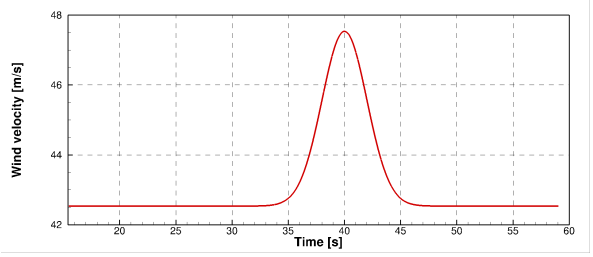

Fig. 8: Perturbation at the inlet: Evolution of the wind velocity versus the time

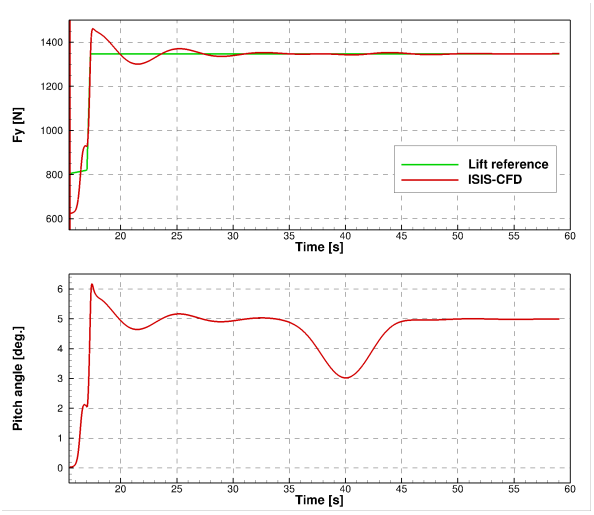

Fig. 9: Perturbation at the inlet: Evolution of lift force (top) and pitch angle (bottom) versus the time

is strongly related to wind velocity. The frequency of 1 Hz remains inside the motor's bandwidth, but at low wind velocity, a strong gain attenuation and phase shift appear. This is highlighted in Fig. 12 where the input-output gains in [dB] with respect to the frequency are given for respectively a wind velocity at 56.7 ms^{-1} in red and at 28.4 ms^{-1} wind in blue. It appears that the cut-off frequency for a wind velocity at 56.7 ms^{-1} is 5 Hz, which is much higher than that for a wind velocity at 28.4 ms^{-1}, which is only of 0.9 Hz. Consequently, Fig. 12 shows that it is illusory to try to compensate for disturbances greater than a few Hertz by pitch variations. Remark that, from the motor point of view, the fast variations in electrical torque are filtered out by the blades inertia and the rotation speed remains constant.

IV. Conclusion

This work presented the control of the aerodynamic lift of a wind turbine blade in a CFD environment, using the ISIS-CFD solver. A model-free based technique has been used to cope with the stabilization of the lift despite the changes of the wind velocity and good tracking performances make this solution very encouraging for further experimental validation. Particularly, future investigations include to evaluate the pertinence of the proposed solution regarding the absorbed energy by the pitch motor as well as develop multiobjective control strategies involving pitch and electrical torque control. From our simulation results, it appears that the pitch control cannot reject a "fast" ($\geq$ 1 Hz) disturbance, so one solution would be to use electrical torque to compensate the "fast" disturbance. Then, the control's objectives are both, to achieve maximum power and also to preserving the integrity of the wind turbine. For that the pitch and electric torque control should be coupled.

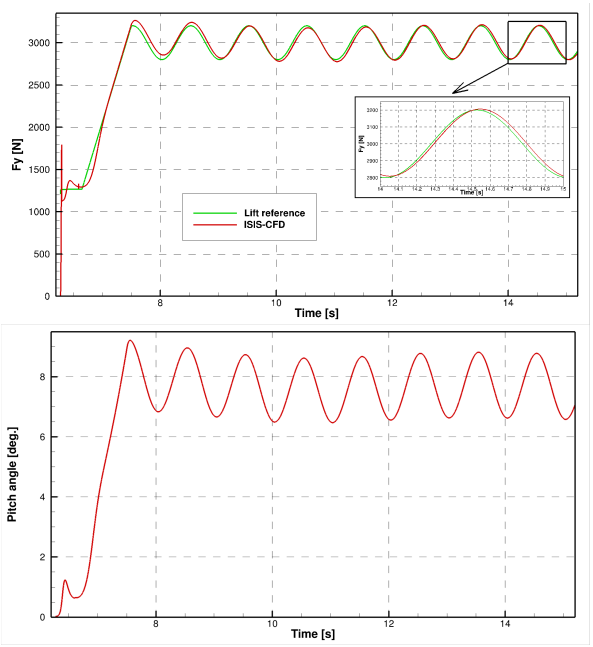

Fig. 10: Sinusoidal F_y^* (f = 1 Hz), Re = 4.70×10^6, U_∞ = 56.7 ms^{-1}: Evolution of lift force (top) and pitch angle (bottom) versus the time

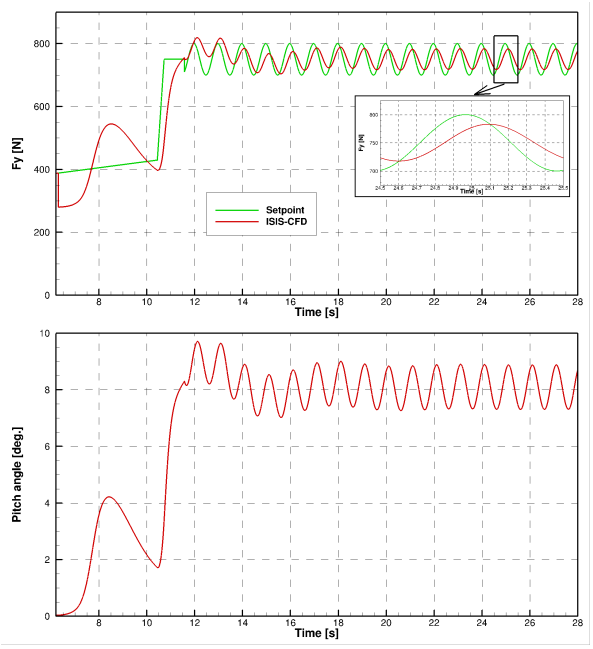

Fig. 11: Sinusoidal F_y^* (f = 1 Hz), Re = 2.35×10^6, U_∞ = 28.4 ms^{-1}: Evolution of lift force (top) and pitch angle (bottom) versus the time

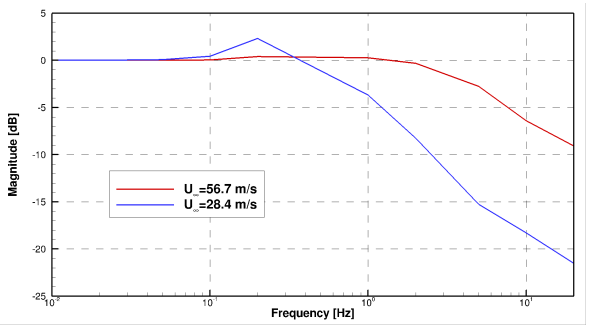

Fig. 12: Frequency response analysis for Re = 2.35×10^6 and 4.70×10^6

REFERENCES

[1] A. Rezaeiha, R. Pereira, and M. Kotsonis, "Fluctuations of angle of attack and lift coefficient and the resultant fatigue loads for a large horizontal axis wind turbine," *Renewable Energy*, vol. 114, pp. 904–916, 2017.

[2] S. Wagner, R. Bareiss, and G. Guidati, *Wind Turbine Noise*. Berlin, Germany: Springer, Feb. 2012.

[3] S. L. Brunton and B. R. Noack, "Closed-Loop Turbulence Control: Progress and Challenges," *Applied Mechanics Reviews*, vol. 67, no. 5, p. 050801, 08 2015.

[4] P. Queutey and M. Visonneau, "An interface capturing method for free-surface hydrodynamic flows," *Computers & Fluids*, vol. 36, no. 9, pp. 1481–1510, 2007.

[5] J. G. Njiri and D. Söffker, "State-of-the-art in wind turbine control: Trends and challenges," *Renewable and Sustainable Energy Reviews*, vol. 60, pp. 377–393, 2016.

[6] H. Jafarnejadsani, J. Pieper, and J. Ehlers, "Adaptive control of a variable-speed variable-pitch wind turbine using radial-basis function neural network," *IEEE Transactions on Control Systems Technology*, vol. 21, no. 6, pp. 2264–2272, 2013.

[7] M. Coquelet, L. Bricteux, M. Moens, and P. Chatelain, "A reinforcement-learning approach for individual pitch control," *Wind Energy*, vol. 25, no. 8, pp. 1343–1362, 2022.

[8] O. Tutty, M. Blackwell, E. Rogers, and R. Sandberg, "Iterative learning control for improved aerodynamic load performance of wind turbines with smart rotors," *IEEE Transactions on Control Systems Technology*, vol. 22, no. 3, pp. 967–979, 2014.

[9] J. E. Sierra-Garcia, M. Santos, and R. Pandit, "Wind turbine pitch reinforcement learning control improved by pid regulator and learning observer," *Engineering Applications of Artificial Intelligence*, vol. 111, p. 104769, 2022.

[10] W. H. Lio, *Blade-pitch control for wind turbine load reductions*, 1st ed., ser. Springer theses. Cham, Switzerland: Springer International Publishing, Mar. 2018.

[11] C. Zhang and F. Plestan, "Individual/collective blade pitch control of floating wind turbine based on adaptive second order sliding mode," *Ocean Engineering*, vol. 228, p. 108897, 2021.

[12] S. Thomsen, H. Niemann, and N. Poulsen, "Individual pitch control of wind turbines using local inflow measurements," *IFAC Proceedings Volumes*, vol. 41, no. 2, pp. 5587–5592, 2008, 17th IFAC World Congress.

[13] B. L. Jones, W. H. Lio, and J. A. Rossiter, "Overcoming fundamental limitations of wind turbine individual blade pitch control with inflow sensors," *Wind Energy*, vol. 21, no. 10, pp. 922–936, 2018.

[14] A. Leroyer and M. Visonneau, "Numerical methods for ranse simulations of a self-propelled fish-like body," *Journal of Fluids and Structures*, vol. 20, no. 7, pp. 975–991, 2005, fluid-Plate Interactions.

[15] E. Guilmineau, G. Deng, A. Leroyer, P. Queutey, M. Visonneau, and J. Wackers, "Assessment of hybrid rans-les formulations for flow simulation around the ahmed body," *Computers & Fluids*, vol. 176, pp. 302–319, 2018.

[16] M. Visonneau, E. Guilmineau, J. Wackers, G. Deng, and P. Queutey, "Assessment of Statistical and Hybrid LES Turbulence Closures for Surface Combatant DTMB5415 at 20° Static Drift Condition," ser. International Conference on Offshore Mechanics and Arctic Engineering, vol. Volume 11: Prof. Robert F. Beck Honoring Symposium on Marine Hydrodynamics, 05 2015, p. V011T12A021.

[17] S. Mozaffari, E. Guilmineau, M. Visonneau, and J. Wackers, "Average-based mesh adaptation for hybrid rans/les simulation of complex flows," *Computers & Fluids*, vol. 232, p. 105202, 2022.

[18] J. Wackers, G. Deng, E. Guilmineau, A. Leroyer, P. Queutey, and M. Visonneau, "Combined refinement criteria for anisotropic grid refinement in free-surface flow simulation," *Computers & Fluids*, vol. 92, pp. 209–222, 2014.

[19] V. Pržulj and B. Basara, "Bounded convection schmes for unstructured grids," in *15th AIAA Computational Fluid Dynamics Conference*, 2001, pp. AIAA–Paper 2001–2593.

[20] C. M. Rhie and W. L. Chow, "A numerical study of the turbulent flow past an isolated aerofoil with trailing edge separation," *AIAA Journal*, vol. 21, pp. 1525–1532, 1983.

[21] R. I. Issa, "Solution of the implicitly discretized fluid flow equations by operator-splitting," *Journal of Computational Physics*, vol. 62, pp. 40–65, 1986.

[22] M. Fliess and C. Join, "Model-free control," *International Journal of Control*, vol. 86, no. 12, pp. 2228–2252, Dec. 2013.

[23] L. Michel, "A para-model agent for dynamical systems," *preprint arXiv*, 2018. [Online]. Available: https://doi.org/10.48550/arXiv.1202.4707

[24] M. Fliess and H. Sira-Ramírez, *Closed-loop Parametric Identification for Continuous-time Linear Systems via New Algebraic Techniques*. London: Springer London, 2008, pp. 363–391.

[25] F. R. Menter, "Two-equation eddy viscosity turbulence models for engineering applications," *AIAA Journal*, vol. 32, pp. 1299–1310, 1994.